Photovoltaic effects on Franz–Keldysh oscillations in photoreflectance spectra: Application to determination of surface Fermi level and surface recombination velocity in undoped Ga As / n-type GaAs epitaxial layer structures

Hideo Takeuchi, Yoshitaka Kamo, Yoshitsugu Yamamoto,

Tomoki Oku, Masahiro Totsuka, Masaaki Nakayama

Citation	Journal of Applied Physics, 97(6); 063708
Issue Date	2005-03-14
Type	Journal Article
Textversion	Publisher
Right	© 2005 American Institute of Physics. This article may be downloaded for personal use only. Any other use requires prior permission of the author and AIP Publishing. The following article appeared in Journal of Applied Physics and maybe found at https://doi.org/10.1063/1.1861968
DOI	10.1063/1.1861968

Self-Archiving by Author(s)

Placed on: Osaka City University Repository

TAKEUCHI, H., KAMO, Y., YAMAMOTO, Y., OKU, T., TOTSUKA, M., & NAKAYAMA, M. (2005). Photovoltaic effects on Franz–Keldysh oscillations in photoreflectance spectra: Application to determination of surface Fermi level and surface recombination velocity in undoped GaAs/n-type GaAs epitaxial layer structures. *Journal of Applied Physics*. 97, 063708.

HTML ABSTRACT + LINKS

JOURNAL OF APPLIED PHYSICS **97**, 063708 (2005)

Photovoltaic effects on Franz–Keldysh oscillations in photoreflectance spectra: Application to determination of surface Fermi level and surface recombination velocity in undoped GaAs/*n*-type GaAs epitaxial layer structures

Hideo Takeuchi,[a] Yoshitaka Kamo, Yoshitsugu Yamamoto, and Tomoki Oku
Microwave Device Development Department, High Frequency and Optical Device Works, Mitsubishi Electric Corporation, 4-1 Mizuhara, Itami, Hyogo 664-8641, Japan

Masahiro Totsuka
Wafer Manufacturing Department, High Frequency and Optical Device Works, Mitsubishi Electric Corporation, 4-1 Mizuhara, Itami, Hyogo 664-8641, Japan

Masaaki Nakayama
Department of Applied Physics, Graduate School of Engineering, Osaka City University, 3-3-138 Sugimoto, Sumiyoshi-ku, Osaka 558-8585, Japan

(Received 23 June 2004; accepted 23 December 2004; published online 14 March 2005)

We demonstrate that the surface Fermi level and surface recombination velocity in undoped GaAs/*n*-type GaAs (*i*-GaAs/*n*-GaAs) epitaxial layer structures can be simultaneously estimated from Franz–Keldysh oscillations (FKOs) in photoreflectance spectra, taking account of the photovoltaic effects. Initially, we performed computational studies on the surface electric fields in *i*-GaAs/*n*-GaAs structures under the illumination of a probe beam. The surface electric-field strength is sensitive to the surface Fermi level and surface recombination velocity. We have found that these parameters can be evaluated from the dependence of the surface electric-field strength on the probe-beam power density. Next, we estimated experimentally the surface Fermi level and surface recombination velocity in an as-grown *i*-GaAs/*n*-GaAs structure by analyzing the photovoltaic effect on the FKOs. The period of the FKOs increases with a decrease in the probe-beam power density. The surface Fermi level and surface recombination velocity are estimated from the probe-beam power dependence of the surface electric-field strength that is obtained from the analysis of the FKOs. We have also applied the analysis of the photovoltaic effect to the assessment of the GaAs surfaces exposed to the nitridation and the catalytic chemical vapor deposition of SiN_x. In addition, we have derived a line-shape function of the FKOs from *i*-GaAs/*n*-GaAs structures, which is applicable even to the FKOs influenced by a probe-beam interference phenomenon in a layered structure. © *2005 American Institute of Physics*.
[DOI: 10.1063/1.1861968]

I. INTRODUCTION

Photoreflectance (PR) spectroscopy has been attracting considerable attention as an optical characterization method for the surface and/or interface of semiconductors.[1,2] The major reason for the attention is the fact that PR spectra are sensitive to the surface and interface electric fields. It is well known that PR spectra from samples with a built-in electric field exhibit oscillatory patterns in the vicinity of the optical transition energies at critical points, the so-called Franz–Keldysh oscillations (FKOs).[1,2] The electro-optic energy, which corresponds to the period of FKOs, is related to the surface and interface electric fields. In compound semiconductors, the surface electric field is produced by surface Fermi-level pinning; therefore, FKOs can be regarded as a measure of the surface Fermi level. For example, Shen *et al.*[3] measured the FKOs appearing in the PR spectra of undoped $Al_xGa_{1-x}As$/*n*-type $Al_xGa_{1-x}As$ (*i*-$Al_xGa_{1-x}As$/*n*-$Al_xGa_{1-x}As$) epitaxial layer structures and deduced the surface Fermi levels of the *i*-$Al_xGa_{1-x}As$ layers. The PR spectra of the *i*-$Al_xGa_{1-x}As$/*n*-$Al_xGa_{1-x}As$ structures usually exhibit clear patterns of the FKOs, leading to the accurate determination of the electric-field strength. Thus, the *i*-$Al_xGa_{1-x}As$/*n*-$Al_xGa_{1-x}As$ structures are often employed in the PR measurements for the characterization of chemically/physically treated surfaces.[4–8]

In order to estimate the surface Fermi level from the FKOs, it has been required to eliminate the photovoltaic effect of a probe beam because it reduces the surface electric-field strength. Consequently, the PR measurements for estimating the surface Fermi level are usually performed using a probe beam with a low power density. In the above-mentioned PR measurements by Shen *et al.*,[3] the probe beam was defocused, so that the power density was less than 0.1 $\mu W/cm^2$. Such a weak probe beam, needless to say, gives rise to remarkable degradation of the signal-to-noise ratio, which results in some difficulty and ambiguity in the PR measurement. It has, therefore, been desired to estimate the surface Fermi level from the FKOs influenced by a rela-

[a]Electronic mail: takeuchi.hideo@lsi.melco.co.jp

 © 2005 American Institute of Physics

tively intense probe beam. In order to make it possible, it is necessary to establish the methodology for the analysis of the photovoltaic effect on FKOs. The analysis will also contribute to the development of the microscopic PR measurement,[9] where the spatial resolution reaches about a few micro meters, so that the photovoltaic effect becomes considerable because of an intense probe-beam power density resulting from a small spot size.

We note that the analysis of the photovoltaic effect has another merit. The photovoltaic effect is brought by photogenerated carriers. Under the continuous illumination of a probe beam, referred to as the steady state, the photogenerated carrier density is determined not only by the power density of the probe beam but also by the lifetime of carriers; therefore, the analysis of the photovoltaic effect can provide the information on the carrier lifetime. In particular, since compound semiconductors have a large density of surface states and surface defects, the lifetime of carriers near the surface is mainly determined by the surface recombination that is characterized by the surface recombination velocity.[10] Consequently, the analysis of the photovoltaic effect on FKOs is applicable to estimate the surface recombination velocity as well as the surface Fermi level. It is noteworthy that the surface recombination velocity correlates with the performance of various semiconductor devices: heterojunction bipolar transistors,[11] laser diodes,[12] solar cells,[13,14] and so on. For example, Ogura and Hsieh[12] reported that the reduction of the surface recombination velocity in surface-emitting laser diodes leads to a low threshold current and an enhancement of the differential quantum efficiency. Thus, the estimation of the surface recombination velocity is important for the development and fabrication of semiconductor devices.

In the present work, we have carried out the analysis of the photovoltaic effect on FKOs appearing in the PR spectra for the purpose of simultaneously determining the surface Fermi level and surface recombination velocity in epitaxial layer structures. At first, we describe the computational studies on the surface electric fields of *i*-GaAs/*n*-GaAs structures. The built-in electric-field strengths at the steady state are calculated using various sets of surface Fermi levels and surface recombination velocities. The systematic results of the calculation indicate that the surface Fermi level and surface recombination velocity can be simultaneously estimated from the dependence of the surface electric-field strength on the probe-beam power density. Next, we estimate experimentally the surface Fermi levels and surface recombination velocities of several *i*-GaAs/*n*-GaAs structures by analyzing the photovoltaic effect on the FKOs. The first sample is an as-grown *i*-GaAs/*n*-GaAs structure. The PR spectra of the as-grown *i*-GaAs/*n*-GaAs structure exhibit a profile consisting of FKOs whose period depends on the probe-beam power density. The dependence of the surface electric-field strength estimated from the FKOs on the probe-beam power density is compared with the calculated results described above. From the comparison, we estimate the surface Fermi level and surface recombination velocity. Furthermore, we also discuss the line shape of the FKOs from the as-grown *i*-GaAs/*n*-GaAs structure, especially focusing on the phase factor. As previously reported,[15,16] the analysis of the phase of FKOs is useful to reduce ambiguity in estimating the electric-field strength. However, the line shape of the FKOs from the *i*-GaAs/*n*-GaAs structure has not been discussed in detail though such a structure has been employed in many studies. Taking account of the spatial distribution of the built-in electric-field strength, the line shape of the FKOs is calculated and compared with the measured spectrum. From the comparison, an appropriate phase factor is derived for a linear plot of the extrema of the FKOs. Next, *i*-GaAs/*n*-GaAs structures with chemically/physically treated surfaces are examined. The two kinds of surface treatments are characterized: the surface nitridation[6,17] and the catalytic chemical vapor deposition (cat-CVD) of SiN_x.[18] The surface nitridation results in a decrease of the period of the FKOs. The surface Fermi level and surface recombination velocity are also estimated in the same manner that is applied to the analysis of the as-grown *i*-GaAs/*n*-GaAs structure. In contrast with the sample exposed to the surface nitridation, after the cat-CVD of SiN_x, the profile of the FKOs exhibits an increase in the period in addition to a phase shift. Taking account of the interference effects of a probe beam in a layered structure, the line-shape function of the FKOs is generalized to the form that is applicable to the FKOs from the *i*-GaAs/*n*-GaAs structures with overlayers. The line shape of the FKOs from the sample covered with the SiN_x film is calculated using the generalized form and compared with the measured spectrum. From the comparison, a generalized phase factor is derived for the linear plot of FKO extrema influenced by the probe-beam interference. Using the linear plot with the generalized phase factor, we estimate the surface electric-field strength, and evaluate the surface Fermi level and surface recombination velocity after the cat-CVD of SiN_x.

II. COMPUTATIONAL STUDIES ON THE SURFACE ELECTRIC FIELD OF *i*-GaAs/*n*-GaAs STRUCTURES

The model structure used in the calculations is an *i*-GaAs/*n*-GaAs $(3.0\times 10^{18}\ \mathrm{cm}^{-3})$, where the value in the parentheses denotes the doping concentration of the *n*-GaAs layer. The *i*-GaAs layer thickness of the model structure is 200 nm, which is the same as that of the samples used in the present experiments. On the other hand, the *n*-GaAs layer thickness of the model structure is different from that of the samples used and is set to be 1.0 μm, because too large a value of the thickness sometimes gives rise to a problem in the convergence of the calculation. Under convergence conditions, we have carefully confirmed that the calculated values hardly depend on the *n*-GaAs layer thickness. The calculations of the built-in electric field and other properties were performed with the use of the computational simulation based on the Boltzmann–Poisson model.[19,20] The parameters employed in the calculations are listed in Tables I and II. Table I denotes the parameters independent of the doping concentration, while the parameters in Table II are doping-concentration dependent. The electron and hole density-of-states masses listed in Table I were applied to the conduction- and valence-band effective densities of states,

TABLE I. Doping-concentration-independent parameters employed in the calculation of the surface electric-field strength in the *i*-GaAs/*n*-GaAs structure.

Parameters	Values
Temperature (K)	300
Photon energy of the probe beam (eV)	1.5
Dielectric constant	13.18[a]
Refractive Index	3.666[b]
Absorption coefficient (cm^{-1})	9030[b]
Electron density-of-states mass	0.067[c]
Hole density-of-states mass	0.547[c]
Intrinsic carrier concentration ($\times 10^6$ cm^{-3})	2.1[d]

[a]Reference 49.
[b]Values at 1.5 eV, Reference 50.
[c]In units of free electron mass, Reference 51. Hole density-of-state mass is calculated from the Luttinger parameters.
[d]Reference 22.

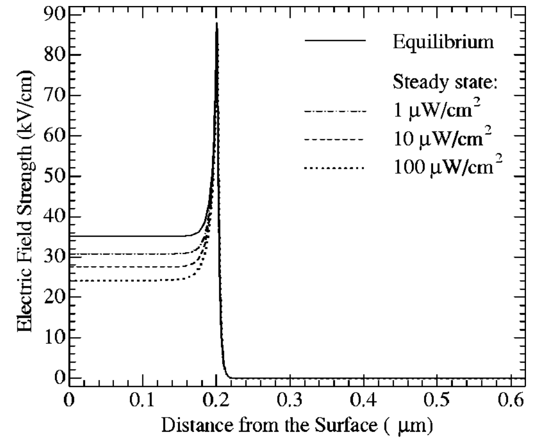

FIG. 1. Calculated built-in electric fields in the *i*-GaAs/*n*-GaAs structure as a function of distance from the surface. The surface Fermi level and surface recombination velocity used are ±0.0 eV and 2.0×10^5 cm/s, respectively. The solid curve corresponds to the equilibrium-state built-in electric field, while the other curves correspond to the steady-state built-in electric fields calculated at the following probe-beam power densities: 1.0 $\mu W/cm^2$ for the dashed-and-dottedcurve, 10 $\mu W/cm^2$ for the dashed curve, and 100 $\mu W/cm^2$ for the dotted curve.

respectively. The band-gap energy $E_{g,n}$ of the *n*-GaAs layer was calculated with the use of the following equations, which take account of the band-gap narrowing induced by the doping effect:[21]

$$E_{g,n} = E_{g,0} - \Delta E_C - \Delta E_T, \qquad (1a)$$

$$\Delta E_C = 2.0 \times 10^{-8} n_{n\text{-GaAs}}^{1/3}, \qquad (1b)$$

$$\Delta E_T = 1.01 \times 10^{-9} n_{n\text{-GaAs}}^{5/12}. \qquad (1c)$$

In Eq. (1a), $E_{g,0}$ and $n_{n\text{-GaAs}}$ denote unperturbed band-gap energy (1.424 eV, according to Ref. 22) and the electron density of the *n*-GaAs layer, respectively. The perturbation terms of ΔE_C and ΔE_T correspond to the band-gap shrinkage due to the exchange-correlation interaction among the free carriers and the band-tailing effect due to the Coulomb interaction of the free carriers with ionized impurities, respectively. It is considered that the band-gap energy changes in accordance with the spatial distribution of the carrier density; however, in the present calculations, the band-gap energy is assumed to be constant in each layer for simplicity because there is large ambiguity in the spatial distribution. In general, bulk carrier lifetimes and mobilities are different from sample to sample. We adopted their appropriate values by referring the several literatures.[22–29] The photon energy of the probe beam is set to be 1.5 eV because that is almost the center energy of the FKOs observed in the PR spectra. Accordingly, the refractive index and absorption coefficient listed in Table I are the values at 1.5 eV. It is known that these optical constants also have a carrier-density dependence; however, the dependence is not taken into account in the calculations for simplicity. The values of the surface Fermi level and surface recombination velocity are specified in each calculation. The recombination at the *i*-GaAs/*n*-GaAs interface is neglected because it is less effective than the surface recombination. The following calculations were carried out using the parameters listed in Tables I and II unless otherwise specified.

TABLE II. Doping-concentration-dependent parameters employed in the calculation of the surface electric-field strength in the *i*-GaAs/*n*-GaAs structure.

	Values	
Parameters	*i*-GaAs layer	*n*-GaAs layer
Band-gap energy (eV)	1.424[a]	1.345[b]
Electron mobility (cm^2/V s)	8000[c]	2100[c]
Hole mobility (cm^2/V s)	400[c]	90[c]
Electron lifetime (ns)	50[d]	50[d]
Hole lifetime (ns)	50[d]	5[d]

[a]Reference 22.
[b]Calculated using Eqs. (1a)–(1c).
[c]References 22–25.
[d]References 26–29.

The one-dimensional built-in electric fields in the *i*-GaAs/*n*-GaAs structure that were calculated at various probe-beam power densities are plotted as a function of distance from the surface in Fig. 1. In the calculations, the surface Fermi level and surface recombination velocity used are ±0.0 eV and 2.0×10^5 cm/s, respectively. Here, the value used for the surface Fermi level is measured from the midgap position. Accordingly, the value of ±0.0 eV means that the surface Fermi level is pinned at the midgap position, while the positive (negative) value corresponds to the situation where the surface Fermi level locates between the conduction-band bottom (valence-band top) and the midgap position. The solid curve in Fig. 1 corresponds to the built-in electric field at the equilibrium state, where the equilibrium state corresponds to the absence of the illumination of the probe beam. On the other hand, the other curves indicate the built-in electric fields at the steady state under continuous illumination conditions. The dashed-and-dotted, dashed, and dotted curves correspond to the built-in electric fields at the probe-beam power densities of 1.0, 10, and 100 $\mu W/cm^2$, respectively. The peaks appearing at 0.2 μm are mainly due to the difference in the band-gap energy between the *i*-GaAs and *n*-GaAs layers resulting from the band-gap shrinkage in the *n*-GaAs layer. Except for the peak, the

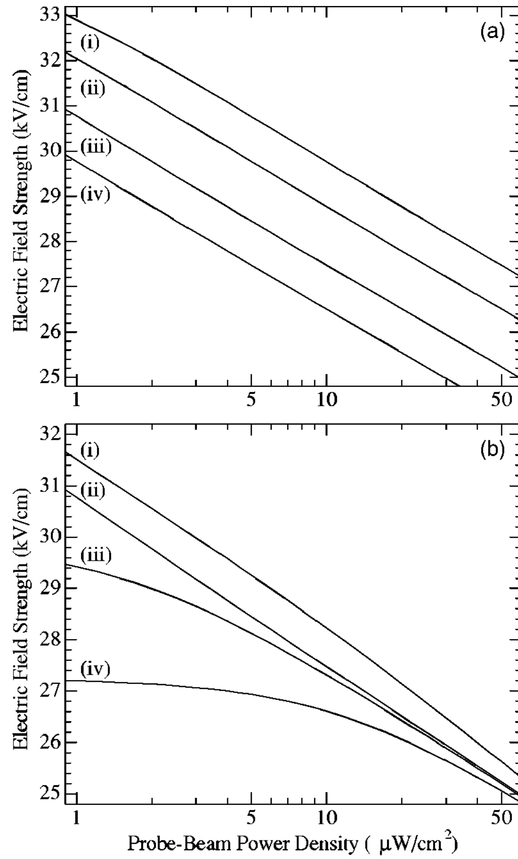

FIG. 2. Calculated surface electric-field strengths in the *i*-GaAs/*n*-GaAs structure as a function of probe-beam power density. (a) Surface electric-field strengths calculated at various surface recombination velocities. The surface recombination velocities used are as follows: 1.0×10^6 cm/s for the curve (i), 5.0×10^5 cm/s for the curve (ii), 2.0×10^5 cm/s for the curve (iii), and 1.0×10^5 cm/s for the curve (iv). The surface Fermi level used for each curve is ±0.0 eV. (b) Surface electric-field strengths calculated at various surface Fermi levels. The surface Fermi levels used are as follows: −0.10 eV for the curve (i), ±0.00 eV for the curve (ii), +0.10 eV for the curve (iii), and +0.15 eV for the curve (iv). The surface recombination velocity used for each curve is 2.0×10^5 cm/s.

built-in electric field uniformly distributes in the *i*-GaAs layer. It is noted that the surface electric-field strength is reduced by the illumination of the probe beam with a power density of μW/cm^2 order, which indicates that the built-in electric field is sensitive to the probe-beam power density. This phenomenon is attributed to the photovoltaic effect on the surface electric field.

In order to investigate the relation among the photovoltaic effect, surface Fermi level, and surface recombination velocity, we calculated the surface electric-field strengths at various probe-beam power densities using various sets of surface Fermi levels and surface recombination velocities. In the calculation, the range of the probe-beam power density is from 0.9 to 60 μW/cm^2, so that it covers the range used in the present experiment: from 2.8 to 30 μW/cm^2. The calculated surface electric-field strengths are plotted as a function of probe-beam power density in Figs. 2(a) and 2(b). In the calculations of the surface electric-field strengths shown in Fig. 2(a), the surface recombination velocity is changed from 1.0×10^5 to 1.0×10^6 cm/s, while the surface Fermi level is fixed to ±0.0 eV. In contrast, in the calculations of the surface electric-field strengths shown in Fig. 2(b), the surface Fermi level is varied from −0.10 to +0.15 eV, while the surface recombination velocity is kept at 2.0×10^5 cm/s. As shown in Fig. 2(a), the surface electric-field strength is enhanced by the increase in the surface recombination velocity. The enhancement of the surface electric-field strength is caused by the suppression of the photovoltaic effect originating from the carriers since the increase in the surface recombination velocity shortens the effective carrier lifetime, which leads to a decrease in the steady-state carrier density. In order to confirm the relation between the carrier density and the surface recombination velocity, we calculated the electron density at the surface. The surface electron densities at the surface recombination velocities of 1.0×10^5 and 5.0×10^5 cm/s are estimated to be 1.2×10^8 and 2.3×10^7 cm^{-3}, respectively, where the calculations were performed using the probe-beam power density of 5.0 μW/cm^2 and the surface Fermi level of ±0.0 eV. This result supports that the carrier density strongly depends on the surface recombination velocity.

Next, we discuss the profiles of the curves in Figs. 2(a) and 2(b) that are obtained by plotting the surface electric-field strength as a function of probe-beam power density. The profile of each curve in Fig. 2(a) indicates that the surface electric-field strength has a linear dependence on the logarithm of the probe-beam power density. In contrast, in Fig. 2(b), the profile of the curve indicates a saturation nature in the regime of the low probe-beam power density as the surface Fermi level approaches to the conduction-band bottom. It is, therefore, concluded that the curve profile is sensitive to the combination of the two parameters: the surface Fermi level and surface recombination velocity. This conclusion means that the surface Fermi level and surface recombination velocity can be simultaneously estimated from the probe-beam power density dependence of the surface electric-field strength.

For the physically meaningful estimation, it is important to clarify the origin of the difference in the curve profile. The difference can be explained on the basis of the theory introduced by Yin *et al.*,[5] which is analogous to the theory on an open circuit photovoltage in solar cells.[30] According to the theory, the steady-state potential barrier height V_B, which corresponds to the potential difference between the Fermi level and the conduction-band bottom under the illumination of the probe light, is written as

$$V_B = V_{B,0} - \frac{\gamma k_B T}{e} \ln\left[\frac{J_{\mathrm{PC}}}{AJ_0(T)} + 1\right], \tag{2}$$

where $V_{B,0}$ is the equilibrium-state potential barrier height, k_B is the Boltzmann constant, T is the temperature, γ is an ideality factor, and A is a geometric factor. The quantities J_{PC} and J_0 are photoinduced and saturation (dark) current densities, respectively. At room temperature, the main contributions to the saturation current density are the thermionic emission and diffusion, while the photoinduced current density is proportional to the probe-beam power density. In the rough approximation, which neglects the Debye-length and the space-charge corrections,[5] the steady-state potential barrier height is given by

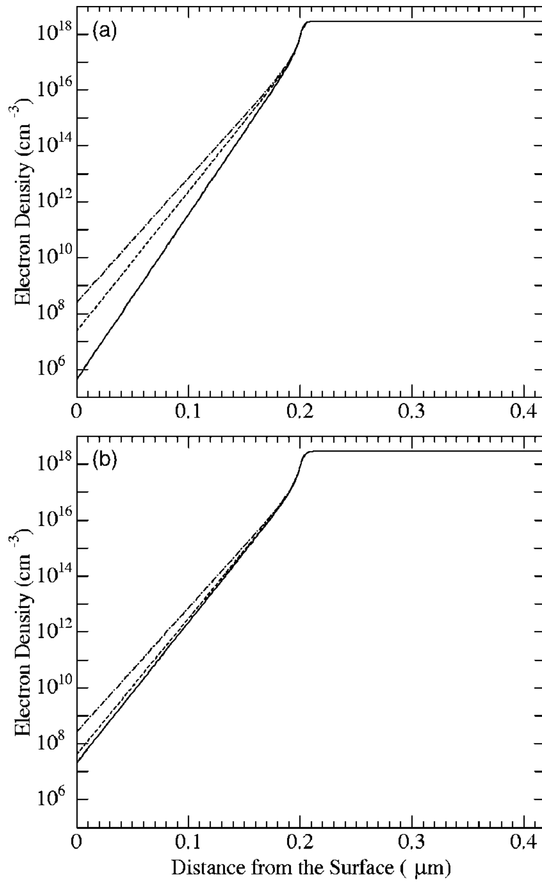

FIG. 3. Calculated electron-density distributions in the i-GaAs/n-GaAs structure at the surface Fermi levels of ±0.0 eV (a) and +0.1 eV (b) as a function of distance from the surface. The surface recombination velocity used is 2.0×10^5 cm/s. Solid curves: equilibrium-state electron-density distribution: Dashed curves: electron-density distribution at the probe-beam power density of 2.0 μW/cm^2. Dashed-and-dotted curves: electron-density distribution at the probe-beam power density of 20 μW/cm^2.

$$V_B = F_s d_{i\text{–GaAs}}, \tag{3}$$

where F_s and $d_{i\text{-GaAs}}$ denote the steady-state surface electric-field strength and the thickness of the i-GaAs layer, respectively. Thus, Eq. (2) can be modified to the following equation:

$$F_s = F_{s,0} - \frac{\gamma k_B T}{e d_{i\text{–GaAs}}} \ln\left[\frac{J_{\text{PC}}}{A J_0(T)} + 1\right]. \tag{4}$$

In the equation, $F_{s,0}$ is the equilibrium-state surface electric-field strength. Apparently, the steady-state surface electric-field strength is proportional to the logarithm of the probe-beam power density in the criterion of $J_0 \ll J_{\text{PC}}$. In contrast, in the criterion of $J_0 \gg J_{\text{PC}}$, the steady-state surface electric-field strength saturates in the regime of the low probe-beam power density. It is, therefore, considered that the linear dependence shown in Fig. 2(a) originates from the former criterion and that the saturation nature shown in Fig. 2(b) arises from the latter criterion.

In order to confirm the above consideration, we investigate the carrier-density distribution. Figures 3(a) and 3(b) show the calculated electron-density distribution as a function of distance from the surface. In the calculations of the electron-density distributions shown in Figs. 3(a) and 3(b), the same surface recombination velocity of 2.0×10^5 cm/s is employed. On the other hand, the different surface Fermi levels are applied to the calculations of the electron-density distributions in Figs. 3(a) and 3(b): ±0.0 and +0.10 eV, respectively. Accordingly, the electron-density distributions in Figs. 3(a) and 3(b) are calculated using the same parameters of the curve (iii) in Fig. 2(a) and those of the curve (iii) in Fig. 2(b), respectively. The solid curves in Figs. 3(a) and 3(b) correspond to the electron-density distributions at the equilibrium state, while the other curves correspond to those at the steady state. In the calculations of the dashed and dashed-and-dotted curves, the probe-beam power densities employed are 2.0 and 20 μW/cm^2, respectively. It is apparent that in the i-GaAs layer the equilibrium-state electron-density distribution is sensitive to the surface Fermi level: the surface electron density shown in Fig. 3(b) is 50 times higher than that shown in Fig. 3(a). This result can be accounted for in terms of the thermal distribution of electrons. Based on the Boltzmann statistics, the equilibrium-state electron density n_s at the surface can be written as

$$n_s = n_{n\text{–GaAs}} \exp\left(-\frac{V_{B,0}}{k_B T}\right). \tag{5}$$

There is a large difference of 0.1 eV between the equilibrium-state potential barrier heights ($V_{B,0}$) corresponding to the surface Fermi levels used in the calculations. According to Eq. (5), at room temperature, the equilibrium-state electron density at the surface shown in Fig. 3(b) is larger by a factor of $\exp(0.1/k_B T) \approx 50$ than that shown in Fig. 3(a), so that the difference in the surface Fermi level is regarded to be responsible for the difference in the electron density.

The photovoltaic effect is suppressed in the situation where the steady-state electron density is comparable to the equilibrium-state electron density, which is suggested by Eq. (2). Figure 3(b) indicates that the illumination of the probe beam with a power density of 2.0 μW/cm^2 results in the slight increase in the electron density. Corresponding to the fact, the curve (iii) in Fig. 2(b) deviates from the linear dependence and begins to saturate in the range of the probe-beam power density lower than 5 μW/cm^2. This is attributed to the above-mentioned situation. On the other hand, in the case where the steady-state electron density is sufficiently higher than the equilibrium-state electron density, the corresponding portions of the curves in Figs. 2(a) and 2(b) exhibit a linear dependence. Thus, the surface Fermi-level dependence of the electron density is attributed to the factor that determines the dependence of the surface electric-field strength on the logarithm of the probe-beam density.

In the present calculations, various parameters, which are listed in Tables I and II, are employed. Among them, the bulk carrier lifetimes and mobilities are sensitive to the sample quality. Surface treatments sometimes unintentionally change these parameters. One may suppose that such changes cause ambiguity in estimating the surface Fermi level and surface recombination velocity. However, the following calculations prove that the surface electric-field strength is insensitive to the changes in the bulk carrier lifetimes and mobilities, which means that the estimation of the surface Fermi level and surface recombination velocity is

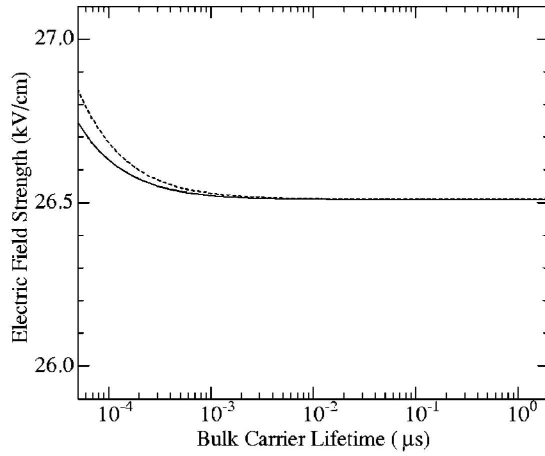

FIG. 4. Calculated steady-state surface electric-field strengths in the i-GaAs/n-GaAs structure as a function of bulk carrier lifetime in the i-GaAs layer. The probe-beam power density, surface Fermi level, and surface recombination velocity applied are 20 μW/cm^2, ±0.0 eV, and 2.0×10^5 cm/s, respectively. The carrier mobilities in the i-GaAs layer employed are as follows: the electron mobility of 8000 (2000) cm^2/V s and hole mobility of 400 (100) cm^2/V s are used for the solid (dashed) curve.

hardly affected by these parameters. At first, we discuss the influence of the bulk carrier lifetimes in the i-GaAs layer. Figure 4 shows the calculated surface electric-field strength as a function of bulk carrier lifetime in the i-GaAs layer. The parameters used are as follows: ±0.0 eV for the surface Fermi level, 2.0×10^5 cm/s for the surface recombination velocity, and 20 μW/cm^2 for the probe-beam power density. The bulk electron and hole lifetimes in the i-GaAs layer are assumed to be the same for simplicity. The solid curve is calculated with the use of the same carrier mobilities listed in Table II. As shown in Fig. 4, the change in the bulk carrier lifetime from 1.0 to 5.0×10^{-5} μs enhances the surface electric-field strength only by 0.24 kV/cm. Because the enhancement corresponds to 0.9% of the value of the surface electric-field strength, the effects of the change in the bulk carrier lifetimes are considered to be negligibly small. This result can be qualitatively explained in terms of the effective carrier lifetime τ_{eff} in the i-GaAs layer, which is given by

$$\frac{1}{\tau_{\text{eff}}} = \frac{1}{\tau_{\text{bulk}}} + \frac{CS}{d_{i\text{-GaAs}}} \quad \text{with } C = 1, \tag{6}$$

where τ_{bulk} and S are the bulk carrier lifetime and the surface recombination velocity, respectively. The second term denotes the effect of the surface recombination. Equation (6) is similar to the equation describing τ_{eff} in Ref. 28. The only difference appears in the coefficient C of the second term, which arises from the fact that the surface recombination is more dominant than the recombination at the opposite interface: the i-GaAs/n-GaAs interface. In the present model structure, using the surface recombination velocity of 2.0×10^5 cm/s, the second term is estimated to be 10 ns^{-1}, which is much larger than the inverse of the bulk carrier lifetime of conventional undoped GaAs crystals. Consequently, the effective carrier lifetime, which affects the carrier density in the i-GaAs layer, is mainly determined by the surface recombination. The electron density in the i-GaAs layer is, therefore, independent of the bulk carrier lifetime, which leads to the conclusion that the surface electric field is insensitive to the change in the bulk carrier lifetime. As shown in Fig. 4, the inverse of the second term (=0.1 ns) almost agrees with the threshold where the surface electric field strength begins to increase. This agreement supports the above-mentioned explanation based on the concept of the effective carrier lifetime.

Next, we discuss the influence of the carrier mobilities in the i-GaAs layer. The dashed curve shown in Fig. 4 is obtained using 2000 and 100 cm^2/V s for the electron and hole mobilities in the i-GaAs layer, respectively. It is obvious that the surface electric-field strength is also insensitive to the changes in the mobilities. This result can be explained in terms of the relation between the photoinduced current density and the carrier mobilities. According to Ref. 31, the relation is expressed by the following equation:

$$J_{\text{PC}} = J_{\text{PC},\infty}\left(1 - \frac{d_{i\text{-GaAs}}^2}{\mu\tau V_{B,0}}\right). \tag{7}$$

The quantity $J_{\text{PC},\infty}$ is the photoinduced current density at the infinite carrier mobilities, while $\mu\tau$ is the average mobility-lifetime product for the electron and hole given by[31]

$$\mu\tau = \frac{2\mu_e\tau_e\mu_h\tau_h}{\mu_e\tau_e + \mu_h\tau_h}, \tag{8}$$

where $\mu_{e(h)}$ and $\tau_{e(h)}$ are the mobility and the bulk carrier lifetime of the electron (hole) in the i-GaAs layer, respectively. Equation (7) indicates that under the finite carrier mobilities the loss of the photoinduced current density occurs owing to the bulk recombination in the i-GaAs layer. It is apparent that the photoinduced current density is independent of the carrier mobilities if the second term is negligibly small. We estimated the denominator of the second term using the following parameters: 2000 cm^2/V s for the electron mobility, 100 cm^2/V s for the hole mobility, 1.0 ns for the bulk carrier lifetimes, and $E_{g,0}/2e$ (=0.712 V) for the equilibrium-state potential barrier height. The value of the denominator is estimated to be 1.4×10^{-7} cm^2, which is much larger than the numerator: the square of the i-GaAs layer thickness (4×10^{-10} cm^2). Consequently, the photoinduced current density is independent of the carrier mobilities and hence the surface electric-field strength is insensitive to the carrier mobilities. Our estimation means that the loss of the photoinduced current density is negligible, which is due to the fact that the thickness of the i-GaAs layer is sufficiently thin.

Finally, we evaluate the accuracy of the present method for estimating the surface Fermi level and surface recombination velocity. It is considered that the accuracy is dominated by the ambiguity in the measured surface electric-field strength. The surface electric-field strength depends on the photon energy of the probe beam owing to a change in photoabsorption even if the probe-beam power density is constant. Consequently, the surface electric-field strength estimated from the FKOs is an average of its values at various photon energies in the spectral range exhibiting the FKOs and hence inevitably accompanies with ambiguity. We calculated the surface electric-field strength in the spectral range

of interest. For example, the surface electric-field strengths calculated at the photon energies of 1.45 and 1.65 eV are 28.5 and 27.9 kV/cm, respectively, where the parameters used are as follows: 5.0 μW/cm^2 for the probe-beam power density, ±0.0 eV for the surface Fermi level, and 2.0×10^5 cm/s for the surface recombination velocity. In the calculation, the surface Fermi level and surface recombination velocity used are typical values in GaAs.[5,32,33] There is a difference of 0.6 kV/cm between the surface electric-field strengths calculated at the photon energies of 1.45 and 1.65 eV. Thus, the calculated results suggest that the surface electric-field strength obtained from the measured FKOs contains ambiguity of ±0.3 kV/cm. We confirmed that the ambiguity of ±0.3 kV/cm hardly depends on the probe-beam power density. We estimated the error of the surface Fermi level resulting from the ambiguity of ±0.3 kV/cm in the surface electric-field strength. As shown in Fig. 2(b), a change in the surface Fermi level remarkably modifies the surface electric-field strength in a regime of the low probe-beam power density; therefore, the error of the surface Fermi level should be determined at the lowest probe-beam power density used in the present measurement. In the present experiment, the lowest probe-beam power density used was 2.8 μW/cm^2. As shown in Fig. 2(b), at the probe-beam power density of 2.8 μW/cm^2, the change in the surface Fermi level from −0.10 to +0.15 eV (the total change of 0.25 eV) reduces the surface electric-field strength by 3.0 kV/cm. As described above, the ambiguity of the surface electric-field strength is ±0.3 kV/cm that is one-tenth of the electric-field strength obtained from the change in the surface Fermi level described above. Thus, the error of the surface Fermi level is estimated to be around ±0.025 eV. We also evaluated the error of the surface recombination velocity. For this purpose, we derived the difference in the surface recombination velocity that produces the change in the surface electric-field strength of ±0.3 kV/cm. For example, the variation in the surface recombination velocity from 2.0×10^5 to 2.4×10^5 cm/s results in the change in the surface electric-field strength from 28.4 to 28.7 kV/cm. In this calculation, the surface Fermi level, probe-beam power density, and photon energy used are ±0.0 eV, 5.0 μW/cm^2, and 1.5 eV, respectively. This result indicates that the change in the surface recombination velocity of 20% leads to the variation in the surface electric-field strength of ±0.3 kV/cm; therefore, the error of the surface recombination velocity is considered to be around 20%. We confirmed that the value of the error ratio hardly depends on the surface recombination velocity. It is noted that the errors estimated above are comparable to the results of the earlier works.[5,32,33] We, therefore, conclude that the present method provides the surface Fermi level and surface recombination velocity with reasonable accuracy.

III. SAMPLES AND EXPERIMENTAL PROCEDURES

The samples used in the PR measurements were three *i*-GaAs(200 nm)/*n*-GaAs(3.0 μm, 3.0×10^{18} cm^{-3}) epitaxial layer structures grown on a 2°-off (001) semi-insulating GaAs wafer by metal organic vapor phase epitaxy, where the values in the parentheses are the individual layer thickness and the doping concentration. One of the epiwafers was examined as an as-grown sample, while the others were exposed to the surface nitridation or cat-CVD of SiN_x. The surface nitridation was performed by annealing the sample in the NH_3 atmosphere. The thickness of the nitrided layer is estimated to be about 2 nm using ellipsometry. The source of the SiN_x film used in the cat-CVD was a mixture of NH_3 and SiH_4, and the tungsten wire was applied to the catalyzer. The thickness and refractive index of the SiN_x film prepared by the cat-CVD are about 50 nm and 2.04, respectively. We carefully checked the difference among the samples and the variation induced by the surface treatment. The sheet resistances of the three epiwafers, which were measured with a contactless conductivity probe before and after the surface treatments, are listed in Table III in addition to the surface electric-field strength of each sample that was estimated from the FKOs before the surface treatment. As shown in Table III, the surface electric-field strengths are the same within the accuracy of the measurements. In addition, the surface treatments hardly produce variation in the sheet resistance, which indicates that the surface treatments do not modify the *n*-GaAs epitaxial layer.

TABLE III. Sheet resistances and surface electric-field strengths of the *i*-GaAs/*n*-GaAs structures before and after the surface treatment.

	Surface electric-field strengths	Sheet resistances	
Surface treatments	Before the treatments (kV/cm)[a]	Before (Ω/sq)[b]	After (Ω/sq)[b]
As grown	26.0±0.2	3.375±0.022	⋯
Surface nitridation	26.2±0.2	3.365±0.019	3.365±0.023
cat-CVD of SiN_x	25.9±0.2	3.369±0.019	3.372±0.020

[a]Estimated from the FKOs measured at the probe-beam power density of 30 μW/cm^2 and the pump-beam power density of 80 mW/cm^2. The values of the average and deviation were obtained from five times measurements at different positions of the wafer.

[b]The values of the average and deviation were obtained from five times measurements at different positions of the wafer.

The PR spectra of the samples were measured at room temperature. In the PR measurement, the pump beam was the laser light with the photon energy of 2.33 eV chopped at the frequency of 2 kHz with an acousto-optic modulator. The power density of the pump beam was 80 mW/cm^2, unless otherwise specified in the following section. The probe beam was obtained from a tungsten–halogen lamp dispersed by a monochromator with a 1.2-nm resolution. In the spectral range of interest, the probe-beam intensity was almost constant and its variation was within 6% of the average. The obtained probe beam was focused onto the sample with the angle of incidence of 15°. The reflected probe beam was detected with a Si photodiode. The dc reflectance component R was recorded by a dc voltmeter, while the modulated reflectance component ΔR of the detected signal was measured using a conventional lock-in technique. The reference phase of the lock-in amplifier was tuned to be in phase with the chopped pump beam.

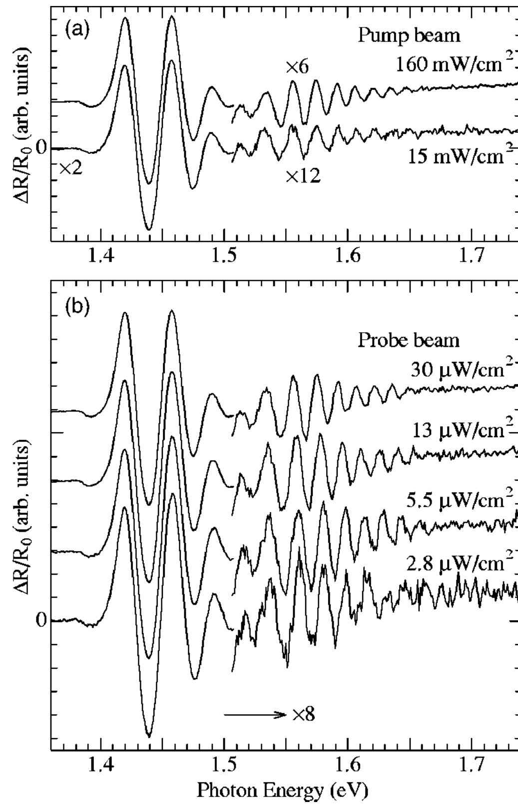

FIG. 5. PR spectra from the i-GaAs(200 nm)/n-GaAs(3.0 μm, 3.0 $\times 10^{18}$ cm^{-3}) structure at room temperature. (a) PR spectra at the pump-beam power densities of 160 and 15 mW/cm^2. The probe-beam power density used is 30 μW/cm^2. (b) PR spectra at various probe-beam power densities. The pump-beam power density used is 80 mW/cm^2.

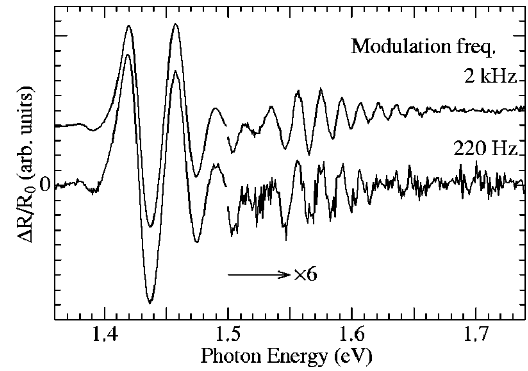

FIG. 6. PR spectra measured at the modulation frequencies of 220 Hz and 2 kHz. The pump- and probe-beam power densities are 80 mW/cm^2 and 30 μW/cm^2, respectively.

IV. EXPERIMENTAL RESULTS AND DISCUSSION

A. FKOs from an as-grown *i*-GaAs/*n*-GaAs structure

The PR spectra from the as-grown i-GaAs/n-GaAs structure are shown in Figs. 5(a) and 5(b). The spectra in Fig. 5(a) were measured at the pump-beam power densities of 15 and 160 mW/cm^2 using the probe beam with a power density of 30 μW/cm^2. In contrast, in the measurement of the spectra shown in Fig. 5(b), the pump-beam power density was kept at 80 mW/cm^2, while the probe-beam power density was varied from 2.8 to 30 μW/cm^2. The spectra shown in both Figs. 5(a) and 5(b) exhibit a large number of oscillations, which are assigned to the FKOs associated with the surface electric field in the i-GaAs/n-GaAs structure.[3] It is noted that the FKOs could not be attributed to those from the interface, taking account of the estimated electric-field strengths that will be discussed later. As shown in Fig. 5(a), the FKOs have the same period regardless of the pump-beam power density. In contrast, as shown in Fig. 5(b), the period of the FKOs increases with a decrease in the probe-beam power density. The pump-beam power density of 80 mW/cm^2 is much higher than that employed in usual PR measurements. It is, therefore, considered that the pump-beam power density is enough to flatten the surface electric field, which is supported by the fact that even the illumination of the beam with a power density of 1.0 μW/cm^2 causes 10% reduction of the surface electric-field strength, as shown in Fig. 1. Consequently, in the present PR measurement, the pump beam modulates the surface electric field from an initial strength in the absence of the pump beam to zero electric field. As a result, the period of the FKOs is sensitive only to the change in the probe-beam power density that dominates the initial electric field.

As mentioned in Sec. III, the modulation frequency used in the present experiment was 2 kHz in order to improve the signal-to-noise ratio. The frequency of 2 kHz is much higher than that used in usual PR measurements: of the order of hundred Hertz. It was reported that the PR signal from an i-GaAs/n-GaAs structure has a time constant around 1 ms.[34] This suggests that the modulation frequency of 2 kHz may be too high to observe an accurate PR signal. In order to clarify the problem of the modulation-frequency effect, it is necessary to check the modulation-frequency dependence of the period of the FKOs. Figure 6 shows the PR spectra measured at 220 Hz and 2 kHz. It is evident that the period of the FKOs at 2 kHz is the same as the period at 220 Hz. This fact indicates that the surface electric field is fully modulated by the pump beam even at 2 kHz; namely, the time constant of the FKO signals is much shorter than 0.5 ms in the present case. According to Ref. 34, the time constant decreases with an increase in the beam power density. The pump-beam power density used in the present experiment is much higher than that used in the experiment of Ref. 34; therefore, it seems that the high power density results in such a short-time constant.

Next, we discuss the line-shape function of the FKOs. The generation mechanism of PR signals arises from the modulation of the dielectric function, which is caused by the intermittent irradiation of the pump beam. The modulated component $\delta\epsilon_{PR}$ of the dielectric function can be written as

$$\delta\epsilon_{PR} = \epsilon_{on} - \epsilon_{off}. \quad (9)$$

In the equation, $\epsilon_{on(off)}$ is the dielectric function of the sample in the presence (absence) of the pump-beam irradiation. In general, the dielectric function of a given layer under the electric field F can be separated into two terms: the component $\epsilon(0)$ independent of the electric field and the component $\langle\Delta\epsilon(F)\rangle$ depending on the electric field.[35]

$$\epsilon_{\mathrm{on(off)}} \approx \epsilon(0) + \langle \Delta\epsilon[F_{\mathrm{on(off)}}] \rangle . \tag{10}$$

In the equation, $F_{\mathrm{on(off)}}$ denotes the electric-field strength in the presence (absence) of the pump-beam irradiation. The generalized form of $\langle \Delta\epsilon(F_i) \rangle$, which is obtained with the use of the Wentzel–Kramer–Brillouin method, is represented by[35]

$$\langle \Delta\epsilon(F_i) \rangle \approx -2ik \int_0^W e^{2ikz} \Delta\epsilon[\hbar\omega, F_i(z)] dz, \tag{11}$$

where z denotes the distance from the surface, W the thickness of a given layer, and k the wave vector of the beam with the photon energy of $\hbar\omega$ in the layer. The quantity $\Delta\epsilon[\hbar\omega, F_i(z)]$ is a perturbation term of the dielectric function, which originates from the presence of $F_i(z)$. For an M_0 critical point, which corresponds to the fundamental transition of GaAs, $\Delta\epsilon[\hbar\omega, F_i(z)]$ is given by[36]

$$\Delta\epsilon(\hbar\omega, F_i) = \frac{B(\hbar\Theta)^{1/2}}{(\hbar\omega)^2}[g(-\eta) + if(-\eta)], \tag{12a}$$

$$\eta \equiv \frac{\hbar\omega - E_{g,0}}{\hbar\Theta}, \tag{12b}$$

$$(\hbar\Theta)^3 \equiv \frac{e^2\hbar^2 F_i^2}{2\mu_r}. \tag{12c}$$

The quantity $\hbar\Theta$ is an electro-optic energy and μ_r is an interband reduced mass in the direction of the electric field, while B is a proportion constant related to the momentum-matrix elements. In Eq. (12a), $f(-\eta)$ and $g(-\eta)$ denote the electro-optic functions consisting of Airy functions.[36] In the PR measurement, the probe beam continuously illuminates the sample. Accordingly, F_{off} corresponds to the electric-field strength under the illumination of the probe beam. In addition, as shown in Fig. 1, the built-in electric field uniformly distributes in the i-GaAs layer. $F_{\mathrm{off}}(z)$ in the i-GaAs layer can, therefore, be written as

$$F_{\mathrm{off}}(z) = F_s = \mathrm{const}. \tag{13}$$

In this equation, F_s is the steady-state surface electric-field strength under the illumination of the probe beam, which is discussed in Sec. II. According to Ref. 35, under the uniform electric field, $\langle \Delta\epsilon(F) \rangle$ can be treated as follows:

$$\langle \Delta\epsilon(F) \rangle = \Delta\epsilon(\hbar\omega, F). \tag{14}$$

Here, we reconsider the photovoltaic effect on the surface electric field. As discussed in Figs. 5 and 6, in the present PR measurements, the pump beam modulates the surface electric field from an initial strength in the absence of the pump beam to zero electric field because of its high power density. The value of $\Delta\epsilon(\hbar\omega, F_{\mathrm{on}})$ can, therefore, be treated as zero. Thus, Eq. (9) can be approximated to

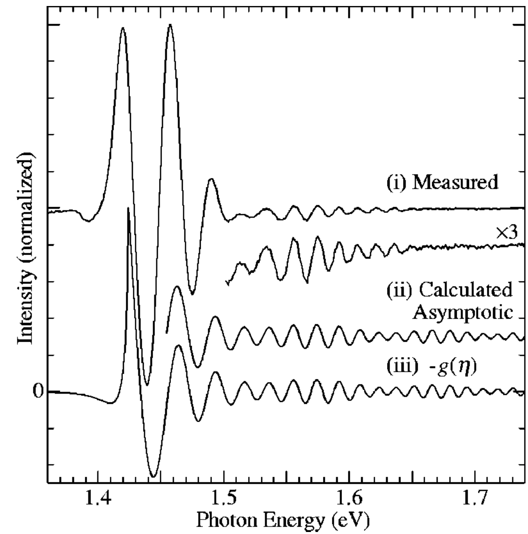

FIG. 7. Comparison between the calculated and measured line shapes of the FKOs from the as-grown i-GaAs/n-GaAs structure. For clarity, each spectrum is normalized. Curve (i): measured PR spectrum at the probe-beam power density of 30 μW/cm^2 and the pump-beam power density of 80 mW/cm^2. Curve (ii): calculated line shape of the FKOs using the asymptotic forms of the electro-optic functions. Curve (iii): calculated line shape of the FKOs consisting of the Γ-HH and Γ-LH components using Eq. (17).

$$\delta\epsilon_{\mathrm{PR}} \approx -\Delta\epsilon(\hbar\omega, F_s) = -\frac{B(\hbar\Theta)^{1/2}}{(\hbar\omega)^2}[g(-\eta) + if(-\eta)]. \tag{15}$$

It is well known that the PR signal is expressed by the following equation:[37]

$$\frac{\Delta R}{R} = \alpha\, \mathrm{Re}[\delta\epsilon_{\mathrm{PR}}] + \beta\, \mathrm{Im}[\delta\epsilon_{\mathrm{PR}}]. \tag{16}$$

The coefficient α and β are the Seraphin coefficients. In the photon-energy range of interest, the values of α and β are positive.[37] In addition, $\beta \ll \alpha$,[37] so that $\Delta R/R$ can be approximated to

$$\frac{\Delta R}{R} \approx -\frac{\alpha B(\hbar\Theta)^{1/2}}{(\hbar\omega)^2} g(-\eta). \tag{17}$$

This equation indicates that the line shape of the FKOs is expressed not by $g(-\eta)$ but by $-g(-\eta)$. The present line-shape function is different from those reported in Refs. 15 and 38, where the built-in electric-field strength of the model structure has a linear dependence on the distance from the surface. According to Ref. 35, the distribution of the built-in electric field affects the mixing of the real and imaginary parts of the perturbation term of the dielectric function through the integration in Eq. (11), which leads to the difference in the line-shape function.

Using the line-shape function derived above, we calculated the line shape of the FKOs. In Fig. 7, the calculated line shape is compared with the PR spectrum measured at the probe-beam power density of 30 μW/cm^2 shown in Fig. 5(b). The calculated line shape is formed by the sum of the Γ-HH and Γ-LH FKO components, taking account of the ratio of the oscillator strength.[39] Here, Γ-HH (Γ-LH) denotes

the heavy-hole-related (light-hole-related) transition at the Γ point. In this calculation, the electron, heavy-hole, and light-hole effective masses used are $0.0665m_0$, $0.34m_0$, and $0.094m_0$, respectively,[40] where m_0 is the electron rest mass in vacuum. The surface electric-field strength used is estimated to be 26.0 kV/cm from a well-established Fourier-transform analysis[41] for the FKOs. The calculated line shape is in phase with the measured spectrum even without any fitting parameters. In Fig. 7, the asymptotic curve of the FKOs, which is derived with the use of the asymptotic forms of the electro-optic functions,[42] is also depicted. As shown in Fig. 7, the asymptotic curve is, of course, in phase with the measured spectrum. The asymptotic curve also consists of the $(\Delta\hat{R}/R)_{\mathrm{HH}}$ and $(\Delta\hat{R}/R)_{\mathrm{LH}}$ of the Γ-HH and Γ-LH components, which are given by

$$\left(\frac{\Delta\hat{R}}{R}\right)_{\mathrm{HH,LH}} \propto \frac{1}{4(\hbar\omega - E_{g,0})(\hbar\omega)^2} \times \cos\left[\frac{4}{3}\left(\frac{\hbar\omega - E_{g,0}}{\hbar\Theta_{\mathrm{HH,LH}}}\right)^{3/2} + \frac{\pi}{2}\right]. \tag{18}$$

In the equation, $\hbar\Theta_{\mathrm{HH(LH)}}$ is an electro-optic energy associated with the Γ-HH (Γ-LH) transition. It is considered that the extrema of the FKOs are mainly determined by the Γ-HH component because the oscillator strength of the Γ-HH transition is three times larger than that of the Γ-LH transition.[39] From Eq. (18), the position $\hbar\omega_j$ of the jth extremum of the asymptotic curve can be obtained as follows:

$$\frac{4}{3}\left(\frac{\hbar\omega_j - E_{g,0}}{\hbar\Theta_{\mathrm{HH}}}\right)^{3/2} + \frac{\pi}{2} = j\pi, \tag{19a}$$

where

$$j = \begin{cases} 1,\ 3,\ 5,\ \ldots, & \text{local-minimum condition.} \\ 0,\ 2,\ 4,\ \ldots, & \text{local-maximum condition.} \end{cases} \tag{19b}$$

This equation can be modified to

$$\hbar\omega_j = \hbar\Theta_{\mathrm{HH}} X_j + E_{\mathrm{g},0}, \tag{20}$$

where X_j is a quasi-index of the jth extremum:

$$X_j = \left[\frac{3\pi}{4}\left(j - \frac{1}{2}\right)\right]^{2/3}. \tag{21}$$

Indeed, several groups[43–45] employed this linear plot based on Eq. (20) by a tacit consent without detailed discussion. At the present stage, where only the FKOs from the as-grown i-GaAs/n-GaAs structure are discussed, the derived linear plot seems to be insignificant. However, the obtained line-shape function can be easily generalized to the form, which can describe the FKOs from the i-GaAs/n-GaAs structure covered with a film. Based on this form, a generalized linear plot can be derived, which will be demonstrated in Sec. IV C.

The extremum positions of the FKOs are plotted according to Eq. (20), as shown in Fig. 8. In this figure, two different linear plots are depicted. The closed circles indicate the linear plot of the extrema of the FKOs in the PR spectrum at the probe-beam power density of 30 μW/cm^2, which is shown in Fig. 5(b). On the other hand, the open circles indicate the linear plot of the FKO extrema in the PR spectrum at the probe-beam power density of 5.5 μW/cm^2. As shown in Eq. (20), the slope of each line is the electro-optic energy, which includes the electric-field strength. The slope of the linear plot indicated by the closed circles yields a value of 26.0 kV/cm for the surface electric-field strength at the probe-beam power density of 30 μW/cm^2. The slope of the linear plot indicated by the open circles is larger than that of the plot indicated by the closed circles. The increase in the slope indicates that the surface electric field is enhanced by the suppression of the photovoltaic effect. It is found that the surface electric-field strength is enhanced to 28.2 kV/cm at 5.5 μW/cm^2. We also estimated the surface electric-field strengths at the other probe-beam power densities. The estimated surface electric-field strengths are plotted in Fig. 9 as a function of probe-beam power density and indicated by the closed circles. From this plot, it is apparent that the surface electric-field strength of the as-grown sample has a linear dependence on the logarithm of the probe-beam power density, which corresponds to the computational results shown in Fig. 2(a). The surface electric-field strengths, which were calculated at the surface Fermi level of ±0.0 eV, are also plotted in Fig. 9. The surface recombination velocity is different in the calculation of each line: the value of 1.0×10^5 cm/s is used for the dashed line, 2.0×10^5 cm/s for the solid line, and 4.0×10^5 cm/s for the dashed-and-dotted line. Comparing the calculated lines with the plot of the surface electric-field strengths obtained from the as-grown sample, the surface Fermi level and surface recombination velocity in the i-GaAs/n-GaAs structure are estimated to be ±0.0 eV and 2.0×10^5 cm/s, respectively. The estimated surface Fermi level agrees with the value reported by Shen *et al.*[3] In addition, the estimated surface recombination velocity is consistent with the reported values.[32,33] Thus, we conclude that the surface Fermi level and surface recombi-

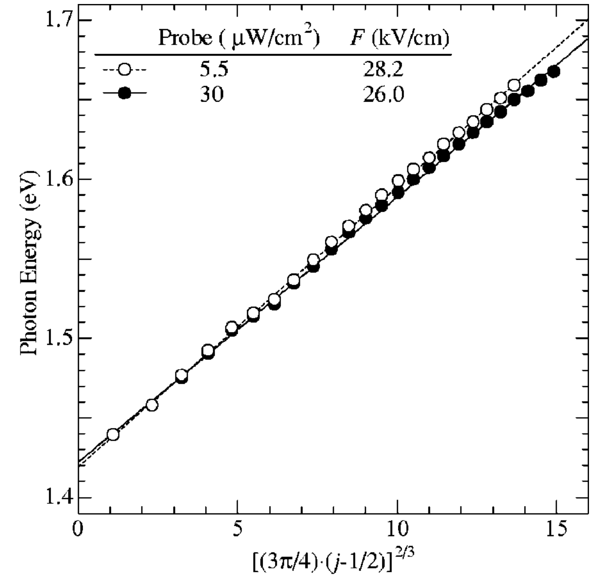

FIG. 8. Linear plot of the extrema of the FKOs shown in Fig. 5(b) according to Eq. (20). The closed and open circles indicate the linear plots of the FKO extrema in the PR spectra measured at the probe-beam power densities of 30 and 5.5 μW/cm^2, respectively.

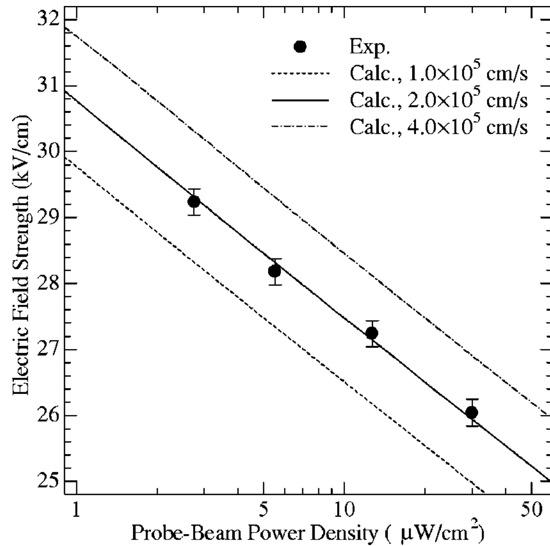

FIG. 9. Comparison between the calculated and estimated surface electric-field strengths with respect to the probe-beam power density. The closed circles indicate the surface electric-field strengths of the as-grown *i*-GaAs/*n*-GaAs structure estimated from the FKOs. The dashed, solid, and dashed-and-solid lines indicate the surface electric-field strengths calculated at the surface Fermi level of ±0.0 eV. The values of the surface recombination velocity employed are as follows: 1.0×10^5 cm/s for the dashed line, 2.0×10^5 cm/s for the solid line, and 4.0×10^5 cm/s for the dashed-and-dotted line.

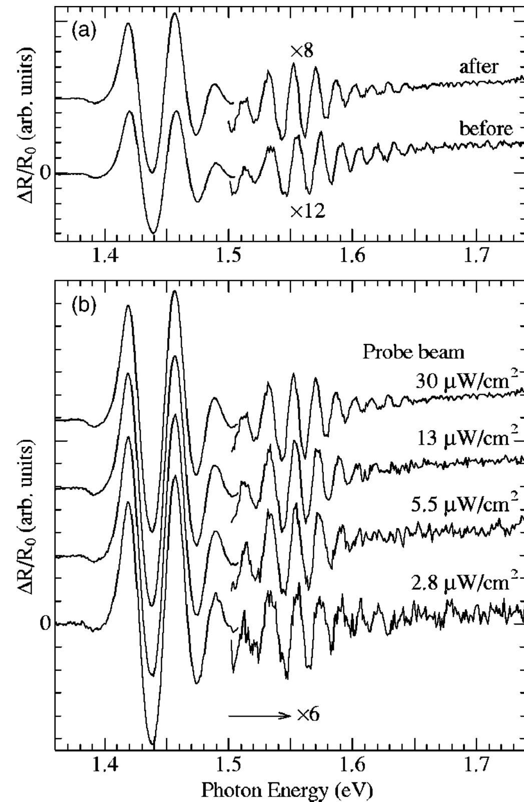

FIG. 10. (a) PR spectra from the *i*-GaAs(200 nm)/*n*-GaAs(3.0 μm, 3.0×10^{18} cm^{-3}) structure before and after the surface nitridation measured at the probe-beam power density of 30 μW/cm^2. (b) PR spectra after the surface nitridation measured at various probe-beam power densities.

nation velocity can be simultaneously determined through the analysis of the photovoltaic effect on the FKOs.

B. Application to the evaluation of the surface nitridation

Figure 10(a) shows the PR spectra from the *i*-GaAs/*n*-GaAs structure before and after the surface nitridation, which were measured at the probe-beam power density of 30 μW/cm^2. In spite of the same measuring condition, the shortening of the period of the FKOs occurs after the surface nitridation; that is, the surface electric-field strength is reduced by the surface nitridation. This result suggests that the surface nitridation changes the surface Fermi level and surface recombination velocity. In order to estimate these parameters, we investigated the dependence of the FKOs on the probe-beam power density. Figure 10(b) shows the PR spectra from the *i*-GaAs/*n*-GaAs structure after the surface nitridation at various probe-beam power densities. The period of the FKOs increases with a decrease in the probe-beam power density; namely, the suppression of photovoltaic effect is also observed in the *i*-GaAs/*n*-GaAs structure after the surface nitridation.

From the FKOs shown in Fig. 10(b), we estimated the surface electric-field strength in the same manner used in Sec. IV A. The estimated surface electric-field strengths are plotted in Fig. 11 as a function of probe-beam power density and indicated by the closed circles. In this figure, the estimated surface electric-field strengths of the as-grown *i*-GaAs/*n*-GaAs structure, which are indicated in the Fig. 9, are replotted as the open circles for a reference. The dashed line indicates the surface electric-field strength that is calculated using the surface Fermi level and surface recombination velocity estimated for the as-grown sample. Comparing the plot indicated by the closed circles with that indicated by the open circles, it is clear that the surface electric-field strength decreases after the surface nitridation. It is, therefore, considered that the surface recombination velocity is reduced by the surface nitridation. In addition, in the regime of the low power density, the estimated surface electric-field strength after the surface nitridation deviates from the linear dependence on the logarithm of the probe-beam power density, which suggests that the surface Fermi level moves from the midgap position. In order to estimate the surface Fermi level and the surface recombination velocity, we calculated the surface electric-field strength. In the calculation, we did not take account of the optical absorption of the nitrided surface because its thickness is negligibly small. The surface electric-field strength, which was calculated using the surface Fermi level of +0.13 eV and the surface recombination velocity of 1.0×10^5 cm/s, is plotted as a solid curve. The solid curve well fits to the experimental values, which indicates that the values of the surface Fermi level and surface recombination velocity used in the calculation are reasonable. The fitting result indicates that the surface Fermi level shifts toward the conduction-band bottom, which means that the equilibrium-state potential barrier height decreases. The decrease in the equilibrium-state potential barrier height enhances to the flow of the electrons toward the surface, which leads to the presumption that the surface recombination velocity is enhanced. Contrary to the presumption, the present estimation indicates that the surface recombination velocity

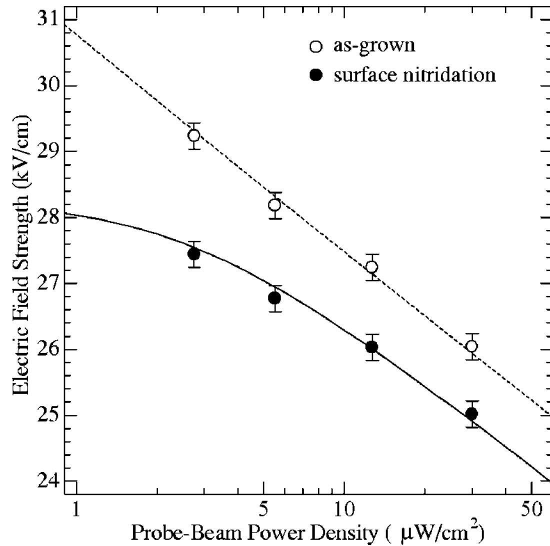

FIG. 11. Comparison between the calculated and estimated surface electric-field strengths with respect to the probe-beam power density. Closed circles: surface electric-field strengths estimated from the FKOs after the surface nitridation. Open circles: replotted surface electric-field strengths of the as-grown i-GaAs/n-GaAs structure shown in Fig. 9. Dashed line: calculated surface electric-field strength using the surface Fermi level of ±0.0 eV and surface recombination velocity of 2.0×10^5 cm/s. Solid curve: calculated surface electric-field strength using the surface Fermi level of +0.13 eV and surface recombination velocity of 1.0×10^5 cm/s.

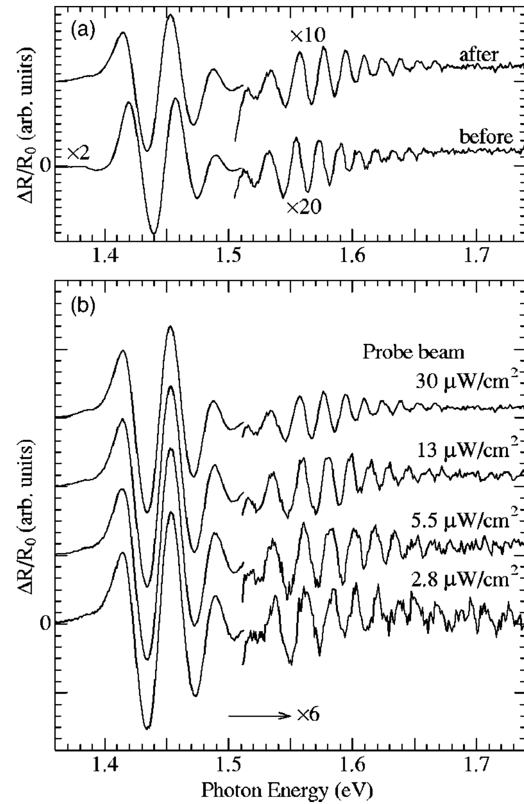

FIG. 12. (a) PR spectra from the i-GaAs(200 nm)/n-GaAs(3.0 μm, 3.0×10^{18} cm^{-3}) structure before and after the cat-CVD of SiN_x measured at the probe-beam power density of 30 μW/cm^2. (b) PR spectra after the cat-CVD of SiN_x measured at various probe-beam power densities.

is reduced by the surface nitridation, where the surface recombination velocity in the as-grown sample is estimated to be 2.0×10^5 cm/s. It is, therefore, considered that the recombination centers at the surface are strongly reduced to exceed the effect of the decrease in the equilibrium-state potential barrier height. Our findings coincide with the previous studies on the surface nitridation. For example, Sun *et al.*[6] evaluated the shift of the surface Fermi level using the PR measurement, which was performed at 420 K to eliminate the photovoltaic effect. They found that the surface Fermi level shifts toward the conduction-band edge after the surface nitridation. Anantathanasarn and Hasegawa[46] measured the photoluminescence from the GaAs epitaxial layer before and after the surface nitridation. From the change in the photoluminescence intensity, they predicted the reduction of the surface recombination velocity after the surface nitridation, which is consistent with the present result, though they did not estimate the value itself. It should be mentioned that the previous studies focused only on the single parameter: either the surface Fermi level or the surface recombination velocity. The evaluation presented here is unique and useful because these parameters can be simultaneously deduced from the same data set obtained from the FKOs.

C. Application to the evaluation of the cat-CVD of SiN_x

Figure 12(a) shows the PR spectra from the i-GaAs/n-GaAs structure before and after the cat-CVD of SiN_x. The spectra were obtained at the probe-beam power density of 30 μW/cm^2. It is noted that the period of the FKOs from the present sample reflects the electric-field strength at the SiN_x/i-GaAs interface because the thickness of SiN_x is not negligible. Consequently, the term "SiN_x/i-GaAs interface electric-field strength" is more suitable than the term "surface electric-field strength" used in the previous subsections. As shown in Fig. 12(a), in the spectrum after the cat-CVD of SiN_x, a large number of the FKOs are observed. In contrast with the FKOs after the surface nitridation, the period of the FKOs after the cat-CVD of SiN_x increases: the SiN_x/i-GaAs interface electric-field strength is larger than the original surface electric-field strength. It is supposed that the increase in the period shifts all of the extrema to the higher-energy side; however, the positions of the extrema do not exhibit such a monotonic shift. The extrema in the energy range less than 1.5 eV move to the lower-energy side, whereas the other extrema shift to the higher-energy side. In general, the positions of the extrema are related not only to the period but also to the phase. Consequently, the observed change in the extremum position suggests that the FKOs exhibit a phase shift. Figure 12(b) shows the PR spectra after the cat-CVD of SiN_x at various probe-beam power densities. The period of the FKOs increases with a decrease in the probe-beam power density, which indicates that the suppression of the photovoltaic effect is also observed in this sample.

In order to analyze the phase shift, we generalize the line-shape function of the FKOs. As previously reported,[15,16] the presence of the overlayer causes the interference of the probe beam, which leads to the phase shift of the FKOs.

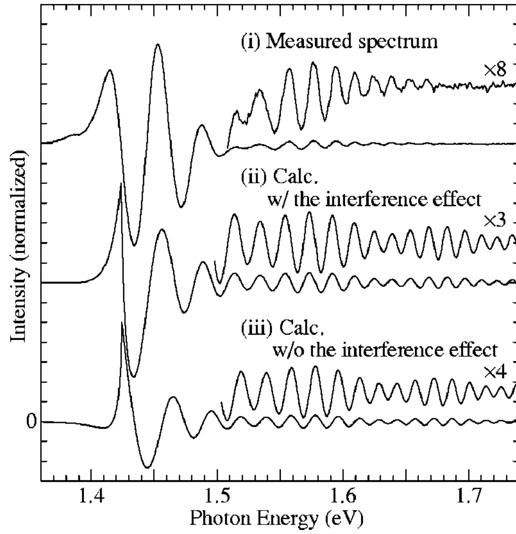

FIG. 13. Comparison between the calculated and measured line shapes of the FKOs. Curve (i): measured PR spectrum after the cat-CVD of SiN_x at the probe-beam power density of 30 $\mu W/cm^2$. Curve (ii): calculated line shape of the FKOs with (w/) taking account of the probe-beam interference effect. Curve (iii): calculated line shape of the FKOs without (w/o) taking account of the probe-beam interference effect.

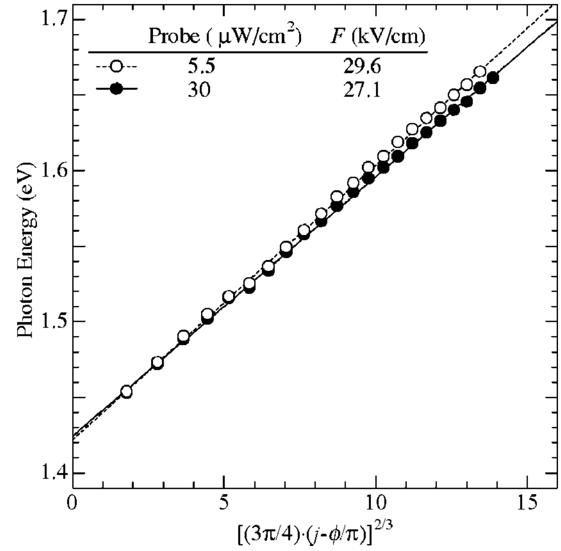

FIG. 14. Linear plot of the extrema of the FKOs after the cat-CVD of SiN_x according to Eq. (25). The closed and open circles indicate the linear plots of the FKO extrema in the PR spectra measured at the probe-beam power densities of 30 and 5.5 $\mu W/cm^2$, respectively.

According to Refs. 15 and 16, in the i-GaAs/n-GaAs structure covered with the SiN_x film, the line-shape function of the FKOs is given by

$$\frac{\Delta R}{R} \propto \mathrm{Re}\{\delta\epsilon_{\mathrm{PR}} \exp[i\delta(\hbar\omega)]\}. \tag{22}$$

In the equation, the quantity $\delta(\hbar\omega)$ denotes the phase delay of the probe beam reflected at the SiN_x film/i-GaAs interface to the probe beam reflected at the surface of the SiN_x film,

$$\delta(\hbar\omega) = 2k_{\mathrm{SiN}_x}(\hbar\omega)d_{\mathrm{SiN}_x}, \tag{23}$$

where d_{SiN_x} and k_{SiN_x} are the thickness and the wave vector of the probe beam in the SiN_x film, respectively. The real projection of $\delta\epsilon_{\mathrm{PR}} \exp[i\delta(\hbar\omega)]$ in Eq. (22) is written as the linear combination of $f(-\eta)$ and $g(-\eta)$, which is formed by the interference-related term $\exp[i\delta(\hbar\omega)]$. In the asymptotic range, the phase of $f(-\eta)$ is different from that of $g(-\eta)$ by $\pi/2$, which leads to the phase shift of the FKOs depending on the thickness of the SiN_x film. The details of the formalism are described in Refs. 15 and 16.

Next, we calculate the line shape of the FKOs using Eqs. (15), (22), and (23) and compare it with the PR spectrum at the probe-beam power density of 30 $\mu W/cm^2$ shown in Fig. 12(b). In advance to the calculation, the Fourier transform of the PR signal was performed to obtain the SiN_x/i-GaAs interface electric-field strength. The SiN_x/i-GaAs interface electric-field strength is estimated to be 26.9 kV/cm. The line shapes of the FKOs, which were calculated using the above-estimated value of the SiN_x/i-GaAs interface electric-field strength, are shown in Fig. 13. In this figure, the two kinds of calculated line shapes are depicted: the line shapes calculated with and without taking account of the interference effect. The line shape of the FKOs calculated with taking account of the interference effect is in phase with the measured spectrum, while the line shape calculated without taking account of the interference effect is out of phase. It is, therefore, confirmed that the generalized line-shape function of the FKOs well explains the profile of the FKOs influenced by the probe-beam interference. Accordingly, the asymptotic form of the Γ-HH FKO component shown in Eq. (18) is generalized to

$$\left(\frac{\Delta\hat{R}}{R}\right)_{\mathrm{HH}} \propto \frac{1}{4(\hbar\omega - E_{g,0})(\hbar\omega)^2} \times \cos\left[\frac{4}{3}\left(\frac{\hbar\omega - E_{g,0}}{\hbar\Theta_{\mathrm{HH}}}\right)^{3/2} + \delta(\hbar\omega) + \frac{\pi}{2}\right]. \tag{24}$$

Thus, the extremum positions of the FKOs can be written as

$$\hbar\omega_j = \hbar\Theta_{\mathrm{HH}}X'_j + E_{g,0}, \tag{25}$$

where X'_j is

$$X'_j = \left[\frac{3\pi}{4}\left(j - \frac{\phi}{\pi}\right)\right]^{2/3}, \tag{26a}$$

$$\phi = \frac{\pi}{2} + \delta(\hbar\omega). \tag{26b}$$

In the equation, the term ϕ can be regarded as a generalized phase factor of the FKOs. We note that the phase of FKOs is also influenced in general by excitonic[47] and surface-termination[48] effects. In addition, the phase depends on the modulation magnitude.[38] Consequently, Eqs. (25), (26a), and (26b) can be applied only to the FKOs from i-GaAs/n-GaAs structures modulated by an intense probe beam used in the present experiment because the effects on the phase of FKOs described above are expected to be considerably reduced.

The extremum positions of the FKOs are plotted according to Eqs. (25), (26a), and (26b), as shown in Fig. 14. The extrema of the FKOs obtained at the probe-beam power density of 30 $\mu W/cm^2$, which are shown in Fig. 12(b), are in-

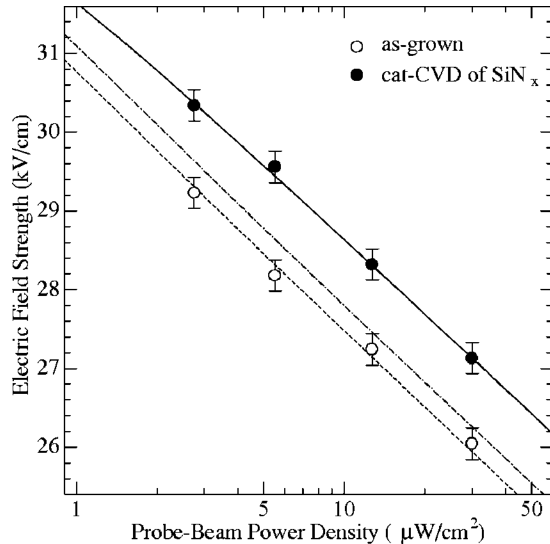

FIG. 15. Comparison between the calculated and estimated surface electric-field strengths with respect to the probe-beam power density. Closed circles: surface electric-field strengths estimated from the FKOs after the cat-CVD of SiN_x. Open circles: replotted surface electric-field strengths of the as-grown *i*-GaAs/*n*-GaAs structure shown in Fig. 9. Dashed line: calculated surface electric-field strength using the surface Fermi level of ±0.0 eV and surface recombination velocity of 2.0×10^5 cm/s. Dashed-and-dotted line: SiN_x/*i*-GaAs interface electric-field strength calculated with taking account of the SiN_x surface reflection effect. The SiN_x/*i*-GaAs interface Fermi level and SiN_x/*i*-GaAs interface recombination velocity used are ±0.0 eV and 2.0×10^5 cm/s, respectively. Solid curve: SiN_x/*i*-GaAs interface electric-field strength calculated with taking account of the change in the Fermi level and recombination velocity at the SiN_x/*i*-GaAs interface in addition to the surface reflection effect. The SiN_x/*i*-GaAs interface Fermi level and SiN_x/*i*-GaAs interface recombination velocity employed are +0.020 eV and 3.8×10^5 cm/s, respectively.

dicated by the closed circles. From the slope of this plot, the SiN_x/*i*-GaAs interface electric-field strength is estimated to be 27.1 kV/cm. The slope of the plot consisting of the open circles, which is obtained from the FKOs measured at the probe-beam power density of $5.5\mu W/cm^2$, indicates that the SiN_x/*i*-GaAs interface electric field is enhanced to 29.6 kV/cm.

The SiN_x/*i*-GaAs interface electric-field strengths at the other probe-beam power densities are also estimated in the same manner and plotted in Fig. 15 as the closed circles. In this figure, the estimated surface electric-field strengths of the as-grown *i*-GaAs/*n*-GaAs structure, which are indicated in the Fig. 9, are replotted as the open circles for a reference. The dashed line indicates the surface electric-field strength that is calculated using the surface Fermi level and surface recombination velocity estimated for the as-grown sample. It is apparent that the SiN_x/*i*-GaAs interface electric-field strength is larger than the surface electric-field strength of the as-grown sample. The following two factors can enhance the electric-field strength. One originates from the reflection of the probe beam at the SiN_x surface. The reflection leads to the reduction of the probe-beam power density at the SiN_x/*i*-GaAs interface and hence the photovoltaic effect is suppressed. Taking account of only this factor, we calculated the SiN_x/*i*-GaAs interface electric-field strength, which is depicted as the dashed-and-dotted line. In the calculation, the Fermi level and recombination velocity at the SiN_x/*i*-GaAs interface employed are the surface Fermi level and surface recombination velocity estimated for the as-grown sample, respectively. In spite of including the reflection effect, the line still deviates from the electric-field strengths obtained from the FKOs. This result suggests that it is necessary to incorporate the other factor: the change in the Fermi level and recombination velocity at the SiN_x/*i*-GaAs interface. The electric-field strength, which was calculated including the above-mentioned change, is depicted as the solid curve. The values of +0.020 eV and 3.8×10^5 cm/s are applied to the Fermi level and recombination velocity at the SiN_x/*i*-GaAs interface, respectively, in order to fit the calculated results to the experimental ones. The present estimation indicates that the Fermi-level pinning is hardly affected by the presence of the SiN_x film, which is consistent with the previous report on the CVD of SiN_x.[7] On the other hand, after the cat-CVD of SiN_x, the SiN_x/*i*-GaAs interface recombination velocity becomes larger than the original value before the cat-CVD. Because the Fermi-level pinning hardly changes, the enhancement of the SiN_x/*i*-GaAs interface recombination velocity suggests that a large amount of the imperfections leading to the recombination are introduced by the cat-CVD of SiN_x. It is usually considered that cat-CVD processes have the advantage of being free from the plasma-related damage. This advantage will lead to the reduction of the surface recombination velocity, so that the cat-CVD of SiN_x can substitute for the conventional plasma-enhanced CVD technology.[18] The present result is contradictory to the usual expectation for the cat-CVD. The clarification of the origin of the imperfections introduced by the cat-CVD is beyond the scope of the present paper.

V. CONCLUSION

We have studied the FKOs in the PR spectra of the *i*-GaAs(200 nm)/*n*-GaAs($3.0\ \mu m, 3.0\times10^{18}\ cm^{-3}$) structures, focusing on the analysis of the photovoltaic effect on the FKOs. In order to clarify the photovoltaic effect on the FKOs, the computational studies on the surface electric field, which is related to the period of the FKOs, have been carried out. It has been found that the built-in electric field is almost uniform in the *i*-GaAs layer. In addition, the built-in electric-field strength is reduced even by the illumination of the probe beam with a power density of $\mu W/cm^2$ order. The calculated surface electric-field strength was plotted as a function of probe-beam power density. It has been found that the surface electric-field strength is sensitive to the surface Fermi level and surface recombination velocity. Furthermore, the profile of the curve that is obtained by the above-mentioned plot can be classified into the following two types. In the first type, the plotted curve has a linear dependence on the logarithm of the probe-beam power density. In the second type, the plotted curve exhibits a saturation nature in the regime of the low probe-beam power density. The above classification is determined by the combination of the values of the surface Fermi level and surface recombination velocity. From these results, we have concluded that the surface Fermi level and surface recombination velocity can be simultaneously estimated from the probe-beam power den-

sity dependence of the surface electric-field strength. The origin of the above-mentioned dependence has been clarified on the basis of the open circuit photovoltage model. Based on the model, the steady-state surface electric field is proportional to the logarithm of the probe-beam power density in the criterion where the photoinduced current density is higher than the saturation current density. In contrast, in the opposite criterion, the steady-state surface electric field saturates in the regime of the low probe-beam power density. In the latter criterion, the steady-state electron density and the equilibrium-state electron density are in the same order, which leads to the high saturation current density comparable to the photoinduced current density. We have also evaluated the accuracy in estimating the surface electric-field strength and surface recombination velocity. The estimated error of the surface Fermi level is around ±0.025 eV, and that of the surface recombination velocity is around ±20% of its value.

Next, we have examined the feasibility of applying the analysis of the photovoltaic effects on the FKOs to the simultaneous determination of the surface Fermi level and surface recombination velocity. At first, the FKOs from the as-grown i-GaAs/n-GaAs structure have been studied. The period of the FKOs increases with a decrease in the probe-beam power density, which reflects the suppression of the photovoltaic effect on the surface electric-field strength. In order to precisely estimate the surface electric-field strength, the phase factor of the FKOs has been discussed in detail. It has been clarified that the line-shape function of the FKOs is expressed by an electro-optic function of $-g(-\eta)$. The calculated line shape is in phase with the measured spectrum. The phase factor, which appears the linear plot for estimating the surface electric-field strength from the FKOs, is derived to be $\pi/2$. The estimated surface electric-field strength has a linear dependence on the logarithm of the probe-beam power density. Comparing the surface electric-field strength obtained from the FKOs with the calculated values, the surface Fermi level and surface recombination velocity are estimated to be 0.00 ± 0.03 eV and $(2.0\pm0.4)\times10^5$ cm/s, respectively, which are consistent with the reported values. We have, therefore, concluded that the surface Fermi level and surface recombination velocity can be determined simultaneously through the analysis of the photovoltaic effect on the FKOs. The analysis has been applied to the assessment of the surface nitridation. After the surface nitridation, the period of the FKOs decreases, which indicates the reduction of the surface electric-field strength. From the dependence of the surface electric-field strength on the probe-beam power density, it has been found that the surface recombination velocity is reduced to $(1.0\pm0.2)\times10^5$ cm/s and that the surface Fermi level shifts by $+0.13\pm0.03$ eV toward the conduction-band bottom from the midgap position. Our findings indicate that the recombination centers at the surface are reduced by the surface nitridation. The effect of the cat-CVD of the SiN_x overlayer has been also evaluated. After the cat-CVD of SiN_x, the FKOs exhibit a phase shift in addition to an increase in the period. The phase shift of the FKOs can be explained by the generalized calculation model for the line shape of the FKOs that takes account of the probe-beam interference effect. The phase of the calculated line shape is in good agreement with that of the measured spectrum. The calculation model provides the generalized linear plot method for the FKO extremum positions. The linear plot has a phase factor related to the phase delay originating from the interference effect. From the electric-field strength estimated with the use of the generalized linear plot, it has been found that after the cat-CVD of SiN_x the recombination velocity at the SiN_x/i-GaAs interface is enhanced to $(3.8\pm0.8)\times10^5$ cm/s in comparison with the original surface recombination velocity before the cat-CVD of SiN_x whereas the Fermi-level pinning hardly changes. This result indicates that the imperfections leading to the recombination are introduced by the cat-CVD of the SiN_x overlayer. Thus, we have reached to the conclusion that the analysis of the photovoltaic effect on the FKOs presented here is useful to evaluate the effects of the chemical and/or physical treatment on the sample surface.

ACKNOWLEDGMENTS

The authors are grateful to Dr. Toshihiro Nakaoka (Research Center for Advanced Science and Technology, The University of Tokyo) for useful discussions.

[1] F. H. Pollak and H. Shen, Mater. Sci. Eng., R. **10**, 275 (1993).
[2] H. Shen and M. Dutta, J. Appl. Phys. **78**, 2151 (1995).
[3] H. Shen, M. Dutta, L. Fotiadis, P. G. Newman, R. P. Moerkirk, W. H. Chang, and R. N. Sacks, Appl. Phys. Lett. **57**, 2118 (1990).
[4] X. Yin, H.-M. Chen, F. H. Pollak, Y. Cao, P. A. Montano, P. D. Kirchner, G. D. Pettit, and J. M. Woodall, J. Vac. Sci. Technol. B **9**, 2114 (1991).
[5] X. Yin, H.-M. Chen, F. H. Pollak, Y. Chan, P. A. Montano, P. D. Kirchner, G. D. Pettit, and J. M. Woodall, J. Vac. Sci. Technol. A **10**, 131 (1992).
[6] J. Sun, L. Zhang, and T. F. Kuech, J. Cryst. Growth **195**, 711 (1998).
[7] H. Shen, W. Zhou, J. Pamulapati, and F. Ren, Appl. Phys. Lett. **74**, 1430 (1999).
[8] P. Jin *et al.*, J. Appl. Phys. **93**, 4169 (2003).
[9] L. Aigouy, F. H. Pollak, and G. Gumbs, Appl. Phys. Lett. **70**, 2562 (1997).
[10] A. S. Grove, *Physics and Technology of Semiconductor Devices* (Wiley, New York, 1967), Chap. 5.
[11] S. Tiwari, D. J. Frank, and S. L. Wright, J. Appl. Phys. **64**, 5009 (1988).
[12] M. Ogura and H. C. Hsieh, IEEE J. Quantum Electron. **32**, 597 (1996).
[13] J. A. Hutchby, Appl. Phys. Lett. **26**, 457 (1975).
[14] R. F. McOuat and D. L. Pulfrey, J. Appl. Phys. **47**, 2113 (1976).
[15] H. Takeuchi, Y. Yamamoto, R. Hattori, T. Ishikawa, and M. Nakayama, Jpn. J. Appl. Phys., Part 1 **42**, 6772 (2003).
[16] H. Takeuchi, Y. Yamamoto, and M. Nakayama, J. Appl. Phys. **96**, 1967 (2004).
[17] E. S. Aydil, K. P. Giapis, R. A. Gottscho, V. M. Donnelly, and E. Yoon, J. Vac. Sci. Technol. B **11**, 195 (1993).
[18] H. Matsumura, Thin Solid Films **395**, 1 (2001).
[19] P. A. Basore, IEEE Trans. Electron Devices **37**, 337 (1990).
[20] D. A. Clugston and P. A. Basore, *Proceedings of the 26th IEEE Photovoltaic Specialists Conference*, Anaheim, CA, 29 September–3 October 1997 (IEEE, Piscataway, NJ, 1997), p. 207.
[21] H. C. Huang, S. Yee, and M. Soma, J. Appl. Phys. **67**, 1497 (1990).
[22] *Semiconductors: Basic Data*, edited by O. Madelung (Springer, Berlin 1996).
[23] B. A. Sanborn, Phys. Rev. B **51**, 14256 (1995).
[24] H. S. Bennett, J. Appl. Phys. **80**, 3844 (1996).
[25] H. S. Sotoodeh, A. H. Khalid, and A. A. Rezazadeh, J. Appl. Phys. **87**, 2890 (2000).
[26] R. K. Ahrenkiel, D. J. Dunlavy, J. Benner, R. P. Gale, R. W. McClelland, J. V. Gormley, and B. D. King, Appl. Phys. Lett. **53**, 598 (1988).
[27] R. K. Ahrenkiel and D. J. Dunlavy, J. Vac. Sci. Technol. A **7**, 822 (1989).
[28] G. B. Lush, H. F. MacMillan, B. M. Keyes, D. H. Levi, M. R. Melloch, R. K. Ahrenkiel, and M. S. Lundstrom, J. Appl. Phys. **72**, 1436 (1992).
[29] W. D. Sun and F. H. Pollak, J. Appl. Phys. **83**, 4447 (1998).

[30]J. Nelson, *The Physics of Solar Cells* (Imperial College, London, 2003), Chap. 1.
[31]J. Merten, J. M. Asensi, C. Voz, A. V. Shah, R. Platz, and J. Andreu, IEEE Trans. Electron Devices **45**, 423 (1998).
[32]C. A. Hoffman, K. Jarašiūnas, H. J. Gerritsen, and A. V. Nurmikko, Appl. Phys. Lett. **33**, 536 (1978).
[33]C. A. Hoffman, H. J. Gerritsen, and A. V. Nurmikko, J. Appl. Phys. **51**, 1603 (1980).
[34]H. Shen, M. Dutta, R. Lux, W. Buchwald, L. Fotiadis, and R. N. Sacks, Appl. Phys. Lett. **59**, 321 (1991).
[35]D. E. Aspnes and A. Frova, Solid State Commun. **7**, 155 (1969).
[36]D. E. Aspnes, Phys. Rev. **153**, 972 (1967).
[37]B. O. Seraphin and N. Bottka, Phys. Rev. **145**, 628 (1966).
[38]H. Shen and F. H. Pollak, Phys. Rev. B **42**, 7097 (1990).
[39]P. K. Basu, *Theory of Optical Processes in Semiconductors* (Clarendon, Oxford, 1997), Chap. 4.
[40]D. F. Nelson, R. C. Miller, C. W. Tu, and S. K. Sputz, Phys. Rev. B **36**, 8063 (1987).
[41]D. P. Wang and C. T. Chen, Appl. Phys. Lett. **67**, 2069 (1995).
[42]D. E. Aspnes, Phys. Rev. B **10**, 4228 (1974).
[43]M. Sydor, N. Jahren, W. C. Mitchel, W. V. Lampert, T. W. Haas, M. Y. Yen, S. M. Mudare, and D. H. Tomich, J. Appl. Phys. **67**, 7423 (1990).
[44]A. C. Han, M. Wojtowicz, D. Pascua, T. R. Block, and D. C. Streit, J. Appl. Phys. **82**, 2607 (1997).
[45]H. Sugiyama, H. Yokoyama, and K. Wada, J. Appl. Phys. **86**, 374 (1999).
[46]S. Anantathanasarn and H. Hasegawa, J. Vac. Sci. Technol. B **19**, 1589 (2001).
[47]F. C. Weinstein, J. D. Dow, and B. Y. Lao, Phys. Rev. B **4**, 3502 (1971).
[48]R. Del Sole and D. E. Aspnes, Phys. Rev. B **17**, 3310 (1978).
[49]S. Adachi, J. Appl. Phys. **58**, R1 (1985).
[50]D. E. Aspnes, S. M. Kelso, R. A. Logan, and R. Bhat, J. Appl. Phys. **60**, 754 (1986).
[51]I. Vurgaftman, J. R. Meyer, and L. R. Ram-Mohan, J. Appl. Phys. **89**, 5815 (2001).